nature climate change

Supplementary information

https://doi.org/10.1038/s41558-026-02598-w

Biochemical remodelling of phytoplankton cell composition under climate change

In the format provided by the authors and unedited

Table of Contents

Supplementary Methods

Dataset

We compiled a dataset of in situ measurements of proteins, carbohydrates, and lipids in particulate organic matter or living phytoplankton, from several sources; we used photic zone measurements from 38 studies, which sampled at different locations between 1978 and 2018. Data was extracted from tables or images using WebPlotDigitizer (https://automeris.io/WebPlotDigitizer/).

For model-data comparison, we formed dimensionless ratios Protein–C:C, Carb–C:C, and Lipid–C:C, from the bulk macromolecular measurements (mostly reported as μg L^{-1}) and the average stoichiometric composition of these macromolecules[108], by dividing each macromolecule by the sum of proteins, carbohydrates, and lipids. If all major macromolecules were not available but particulate organic carbon (POC) was reported, values were normalized to the sum of POC.

Another data source is field samples of protein, RNA, and DNA collected from 7 research cruises conducted by the Bedford Institute of Oceanography, Canada, starting in September 1978 and ending in July 1981 (Table S1)[45–48,100–102]. Samples were taken from different locations with Niskin bottles, filtered (membrane or glass fiber filters depending on station), stored at –20°C, and analyzed fluorometrically to quantify RNA, DNA, and proteins. The methodology remained largely consistent across these 12 reports. In order to match these values with our study, we converted the measurements to Protein–C:C, RNA–C:C, and DNA–C:C, and estimated Carb–C:C and Lipid–C:C using the relationship:

$$\text{Carb–C:C} + \text{Lipid–C:C} = 1 - [\ \text{Protein–C:C} + \text{RNA–C:C} + \text{DNA–C:C}\ ].$$

We excluded outliers that were outside of ± 2 std of the mean (n_{outliers}=10), and defined the Arctic as all regions north of 66°N. After the removal of outliers, there were 298 observations of Protein–C:C, and Carb–C:C plus Lipid–C:C from the Bedford Institute of Oceanography.

Data distributions, data sources, and further information on sampling date and geographic locations are summarised in Table S1.

Statistical analyses

To examine macromolecular changes over time, we applied linear regressions of the macromolecules vs. time in the Arctic and the Antarctic (Figure 3c–f, Extended Data Fig. 8). These regressions were obtained by the following procedure: Carb–C and Lipid–C were summed. After $\log_{10}$ transforming the

ratios, we removed the outliers (values that were farther than 1.5 times the interquartile range from the median). We did this on log scale, as the data were non-negative and right skewed. We fitted linear regression to the data and recorded the p-value and R^2. For linear regression data obtained only with colorimetric methods, see Table S5. For data obtained with isotope labelling and colorimetric methods, see Table S6.

Comparison of modeled macromolecular allocation with observations

Most of the data in the compiled data is from polar regions, the Japan Sea, or other restricted basins or coastal environments (Table S1). This challenges a point-by-point comparison to our coarse-resolution model, which does not resolve restricted basins, coastal environments or riverine sources. Within the data compilation we identified three studies across open-ocean gradients[27,29,30] and compare modeled and observed trends along these transects. We extracted the data from Liefer et al., 2024 from Supplementary Table S3. We divided the values of protein, carbohydrates, and lipids by macromolecular carbon. To compare with the model, we retrieved the simulated cellular allocation to protein, carbohydrates, lipids, chlorophyll, nucleic acids (DNA+RNA), at each location where a measurement was made (10 m depth-integrated mean) at model output average (years 2010–2020) and plotted against latitude (Extended Data Figure 2). In the case of Handa et al., 1973 numeric values were unavailable in tables, and we extracted euphotic zone data from Figures 1, 6b, and 7b using WebPlotDigitizer. We extracted the model output of Protein–C:C, Carb–C:C, and temperature from the pre-industrial simulation at each longitude and latitude, and a measurement (0–115m depth-integrated value) was made and plotted against SST for comparison. To compare the model output with the Handa and Tanoue 1988 we extracted the data on Protein–C:C, Carb–C:C and Lipid–C:C from Table 1 (only data from the upper 100m). We conducted a point-by-point comparison to the depth-integrated (0–115m) preindustrial values.

Comparison of modeled C:N:P_{org} with observations

Dataset of in situ elemental composition of organic matter from 1974–2020[31–33] were analyzed to assess the distribution of particulate organic matter C:N_{org}, C:P_{org} and N:P_{org} ratios across 17 ecological provinces defined by SST, chlorophyll a concentrations, ice fraction, and maximum mixed layer depth[34] (Extended Data Figure 3). We included only samples from the surface (0–170 m) in the analysis and excluded samples where POP was lower than 5 nM, as this was the reported practical detection limit[31].

Furthermore, we included only open ocean samples, where the bathymetric depth was deeper than 1 km, and ecoprovinces, where observations exceeded 15. This screening yielded 15,012, 5,442, and 5,658 observational data points of $C:N_{org}$, $C:P_{org}$, and $N:P_{org}$, respectively. Modeled $C:N_{org}$, $C:P_{org}$, and $N:P_{org}$ values (pre-industrial equilibrium conditions) were extracted for grid cells corresponding to each ecological region, integrated over sampling depth. The observational and modeled data's 25th, 50th (median), and 75th percentiles were recorded (Fig. S2–Fig. S4, Table S2–Table S4).

To compare the model and observations, data at each ecoprovince were log-transformed (base-10). A normal distribution was fitted to the log-transformed observed and modeled data, and the mean (μ) was extracted (Table S4). To quantify the relative differences between observed and modeled distributions, the percentage difference between the means of the distributions was calculated for each province using the following formula:

$$\sigma = \frac{|(C:P)_j' - (C:P)j\ |}{(C:P)j} \cdot 100, \qquad \textit{Eq. S1}$$

where $(C:P)_j'$ is the modeled value and $(C:P)_j$ is the observed value in ecoprovince j. A Kolmogorov-Smirnov (KS) test was performed to evaluate the similarity between the cumulative distribution functions of the observed and modeled data, with the KS statistic representing the maximum difference recorded (Table S4).

Calculation of the caloric content of organic matter

Following the widely used method for estimating the energy contents in human food[26], the caloric energy content can be determined by the composition of the major macromolecules in the cell, mainly proteins, carbohydrates, and lipids, which account for >95% of cellular carbon[6]. Lipids contain 9.50 kcal/g, while proteins and carbohydrates contain 4.20 and 4.19 kcal/g, respectively[26]. Using these values and model estimates of macromolecular mass in phytoplankton under different environmental conditions, we estimate the global energy content in phytoplankton.

The caloric content of organic matter (Q_{Cal}^{C}; kcal/gC) was estimated using the following equation:

$$Q_{\mathrm{cal}}^{\mathrm{C}} = Q_{\mathrm{Cal}}^{\mathrm{Pro}} + Q_{\mathrm{Cal}}^{\mathrm{Carb}} + Q_{\mathrm{Cal}}^{\mathrm{Lip}} \qquad \textit{Eq. S2}$$

where:

$$Q_{\mathrm{Cal}}^{\mathrm{Pro}} = \frac{Q_{\mathrm{C}}^{\mathrm{Pro}}\ \mathrm{mol\ C\ in\ proteins}}{\mathrm{mol\ C}} \cdot \frac{100\ \mathrm{g\ proteins}}{4.43\ \mathrm{mol\ C\ proteins}} \cdot \frac{\mathrm{mol\ C}}{12\ \mathrm{g\ C}} \cdot \frac{4.19\ \mathrm{kcal}}{\mathrm{g\ proteins}} \qquad \textit{Eq. S3}$$

$$Q_{\mathrm{Cal}}^{\mathrm{Carb}} = \frac{Q_{\mathrm{C}}^{\mathrm{Carb}}\ \mathrm{mol\ C\ in\ carbs}}{\mathrm{mol\ C}} \cdot \frac{180\ \mathrm{g\ carbs}}{6.0\ \mathrm{mol\ C\ carbs}} \cdot \frac{\mathrm{mol\ C}}{12\ \mathrm{g\ C}} \cdot \frac{4.20\ \mathrm{kcal}}{\mathrm{g\ carbs}} \qquad \textit{Eq. S4}$$

$$Q_{\mathrm{Cal}}^{\mathrm{Lip}} = \frac{Q_{\mathrm{C}}^{\mathrm{Lip}}\ \mathrm{mol\ C\ in\ lipids}}{\mathrm{mol\ C}} \cdot \frac{634\ \mathrm{g\ lipids}}{40\ \mathrm{mol\ C\ lipids}} \cdot \frac{\mathrm{mol\ C}}{12\ \mathrm{g\ C}} \cdot \frac{9.50\ \mathrm{kcal}}{\mathrm{g\ lipids}} \qquad \textit{Eq. S5}$$

Here $Q_{\mathrm{C}}^{\mathrm{Pro}}$, $Q_{\mathrm{C}}^{\mathrm{Carb}}$, and $Q_{\mathrm{C}}^{\mathrm{Lip}}$ are cellular allocations of carbon to proteins, carbohydrates, and lipids, respectively, derived from model simulations averaged over depth (0–170 m) in preindustrial simulations. 100, 180, 634 are the molecular weights (g/mol) of proteins, carbohydrates, and lipids for 4.43, 6.0, and 40 mol C in these molecules respectively[108]. 4.19, 4.20, and 9.50 kcal/g are conversion factors from kcal/g for proteins, carbohydrates, and lipids, respectively.

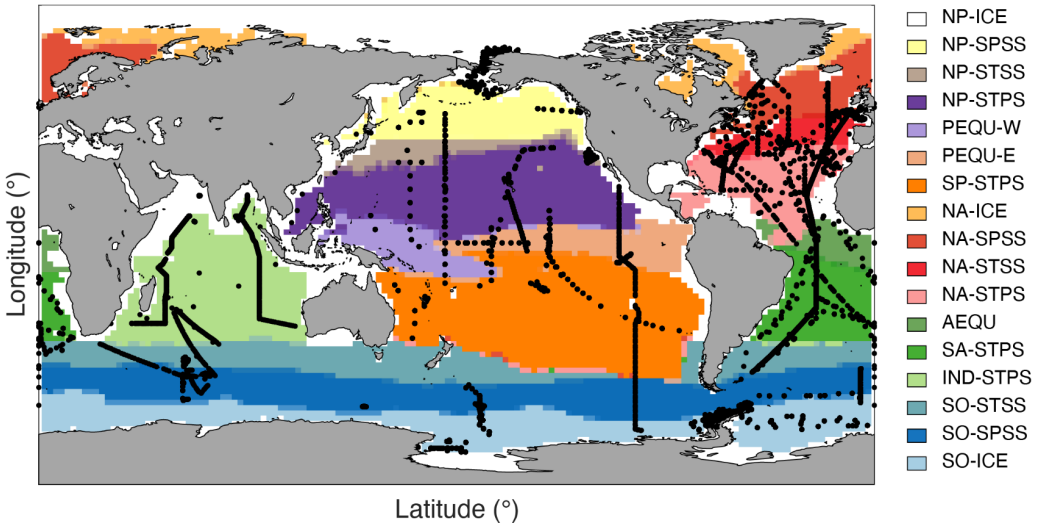

Fig. S1: Sampling locations of particulate organic matter $C:N_{org}$, $C:P_{org}$, and $N:P_{org}$ across global ecoprovinces. Sampling locations[31,33] (black dots) of $C:N_{org}$, $C:P_{org}$, and $N:P_{org}$ plotted against ecoprovinces defined by SST, chlorophyll a concentrations, ice fraction, and maximum mixed layer depth[34]. Only locations meeting two criteria are included: (1) bathymetric depth greater than 1 km (open ocean) and (2) sampling conducted within the upper 170 m, corresponding to the mixed layer. Regions: NP-ICE: North Pacific Ice, NP-SPSS: North Pacific Subpolar Seasonally Stratified, NP-STSS: North Pacific Subtropical Seasonally Stratified, NP-STPS: North Pacific Subtropical Permanent Stratified, PEQU-W: West Pacific Equatorial, PEQU-E: East Pacific Equatorial, SP-STPS: South Pacific Subtropical Permanent Stratified, NA-ICE: North Atlantic Ice, NA-SPSS: North Atlantic Subpolar Seasonally Stratified, NA-STSS: North Atlantic Subtropical Seasonally Stratified, NA-STPS: North Atlantic Subtropical Permanent Stratified, AEQU: Atlantic Equatorial, SA-STPS: South Atlantic Subtropical Permanent Stratified, IND-STPS: Indian Ocean Subtropical Permanent Stratified, SO-STSS: Southern Ocean Subtropical Seasonally Stratified, SO-SPSS: Southern Ocean Subpolar Seasonally Stratified, SO-ICE: Southern Ocean Ice.

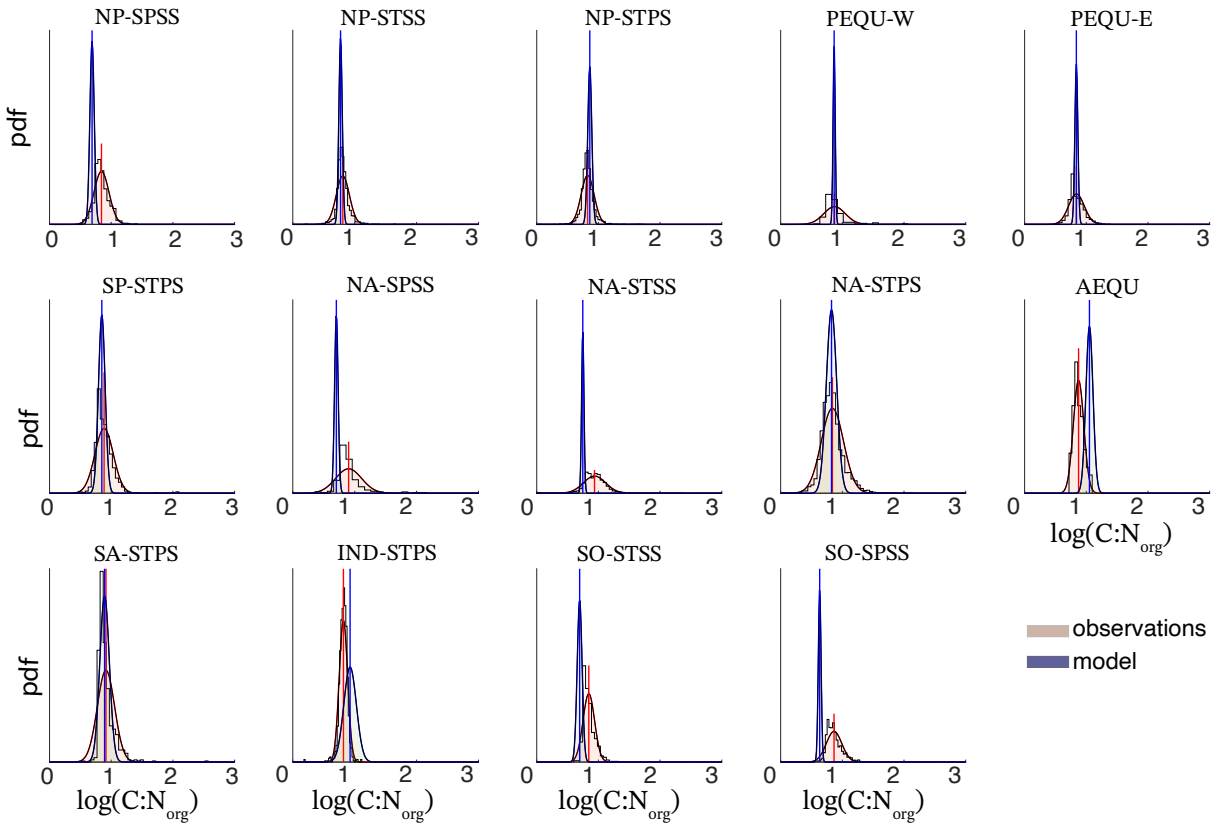

Fig. S2: Comparison between modeled and observed C:N$_{org}$ distributions. The orange Probability Density Functions (PDFs) represent the observed log-transformed C:N$_{org}$ ratios, while the blue pdfs represent the log-transformed modeled C:N$_{org}$ ratios calculated from the macromolecular model (molar ratios). The vertical lines represent the means of the distributions. All data were clustered according to oceanographic regions defined in Fig. S1.

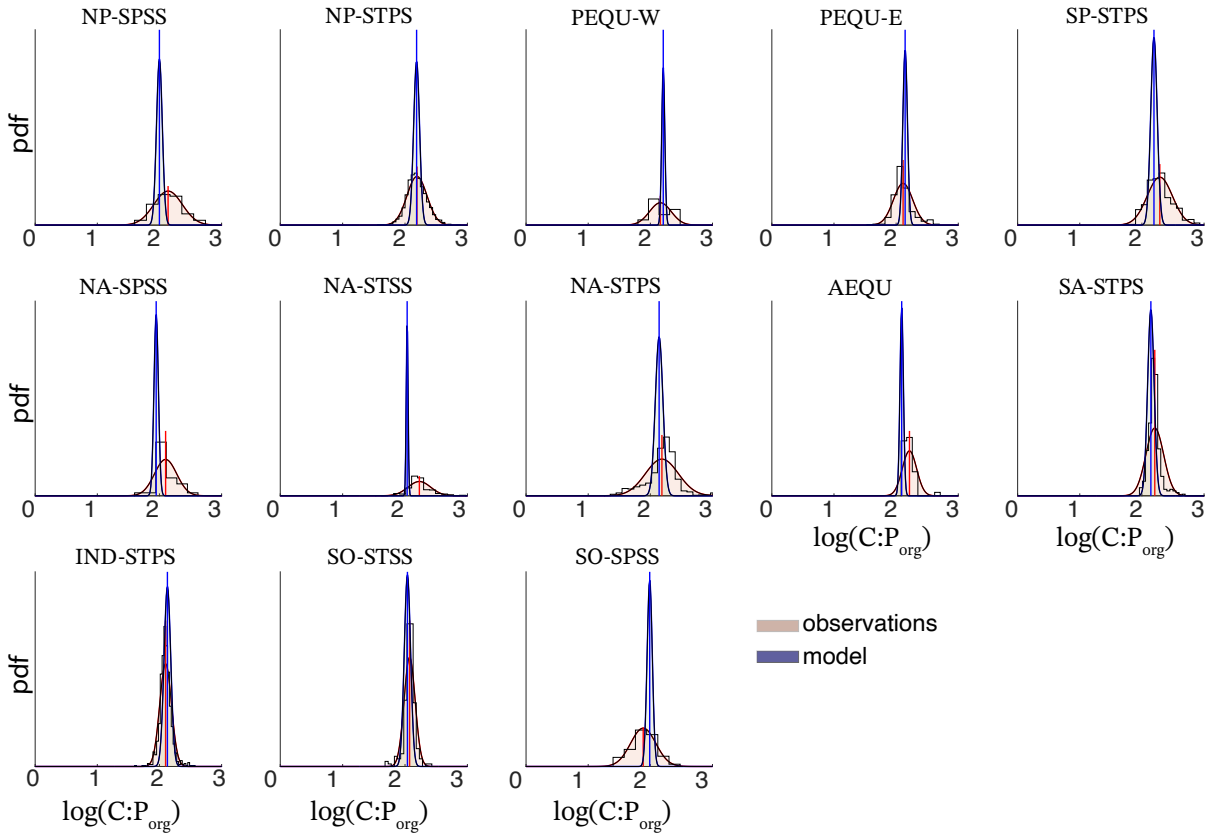

Fig. S3: Comparison between modeled and observed C:P_{org} distributions. The orange Probability Density Functions (PDFs) represent the observed log-transformed C:P_{org} ratios, while the blue pdfs represent the log-transformed modeled C:P_{org} ratios calculated from the macromolecular model (molar ratios). The vertical lines represent the means of the distributions. All data were clustered according to oceanographic regions defined in Fig. S1.

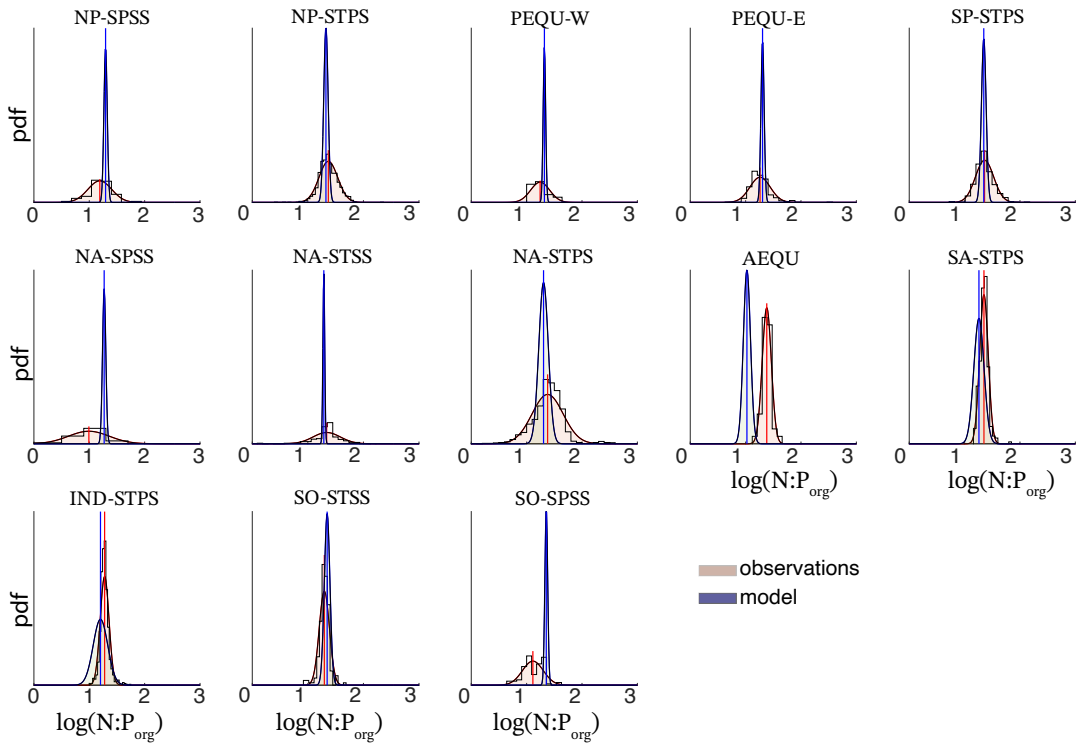

Fig. S4: Comparison between modeled and observed N:P_{org} distributions. The orange Probability Density Functions (PDFs) represent the observed log-transformed N:P_{org} ratios, while the blue pdfs represent the log-transformed modeled N:P_{org} ratios calculated from the macromolecular model (molar ratios). The vertical lines represent the means of the distributions. All data were clustered according to oceanographic regions defined in Fig. S1.

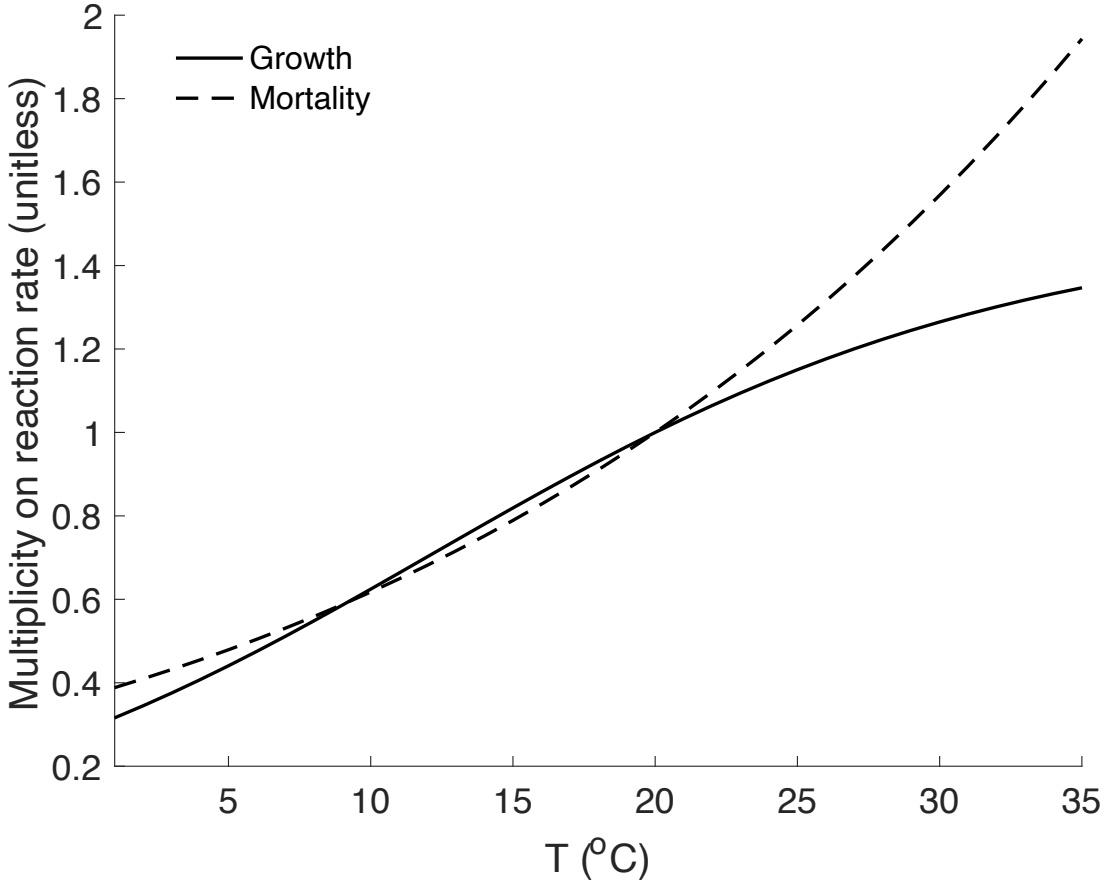

Fig. S5: The effect of temperature on phytoplankton growth and mortality rates. We calculated the temperature response on growth from the carbon mass balance (Eq. 1). Mortality follows an Arrhenius relationship with an activation energy of 34,000 J/mol[76].

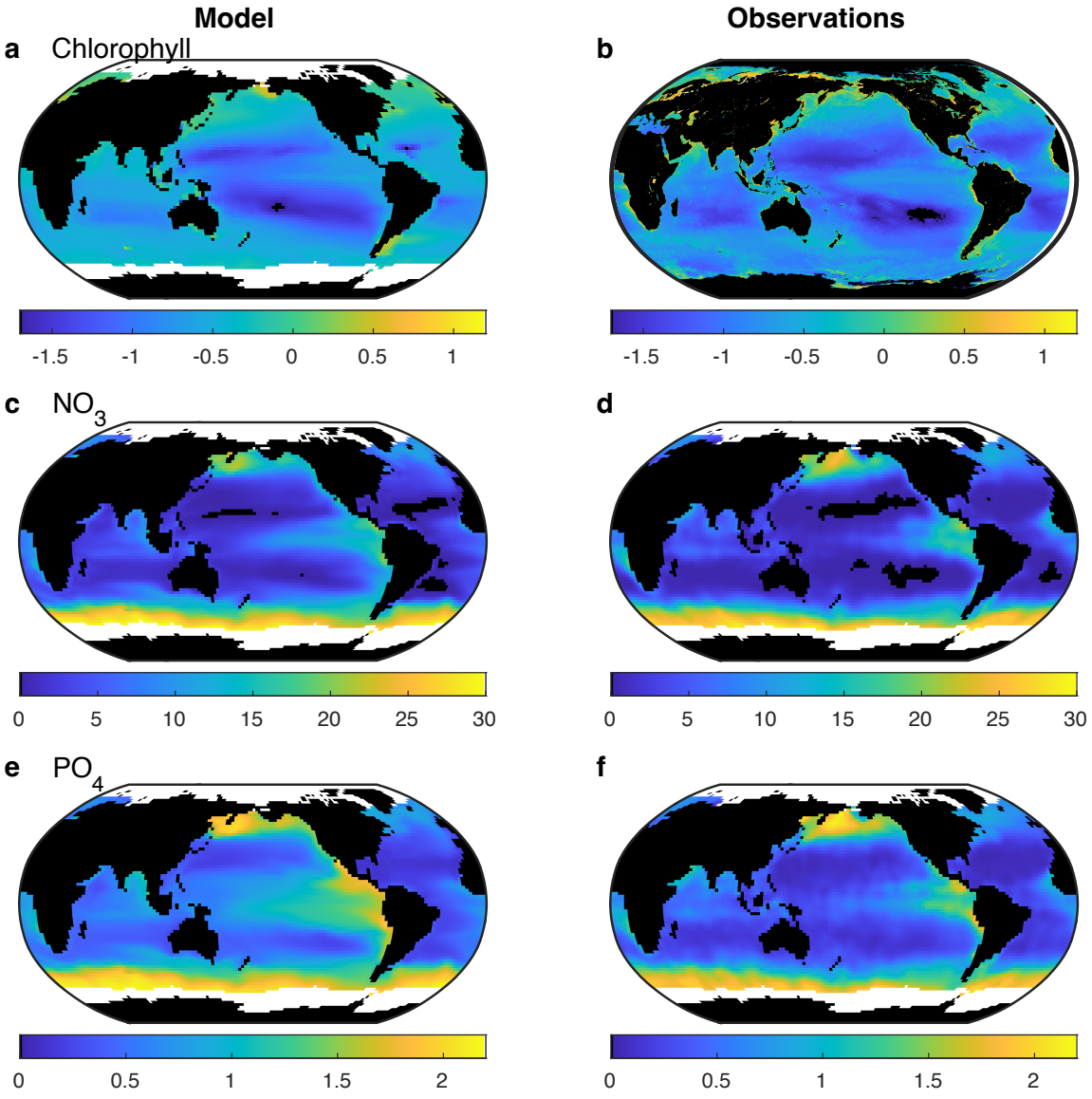

Fig. S6: Comparison between observed and modeled biogeochemical tracers. Depth-integrated (0–115 m), annual means of (**a**, **b**) chlorophyll concentration (mg Chl m^{-3}) (**c**, **d**) nitrate (mmol m^{-3}), and (**e**, **f**) phosphate (mmol m^{-3}). Observed chlorophyll data are derived from ocean colour products[109], while dissolved nutrient observations are from the World Ocean Atlas[110]. The left column shows model results, and the right column shows observational data. The model results represent a 10-year mean of the model output for the preindustrial simulation (Phase 1).

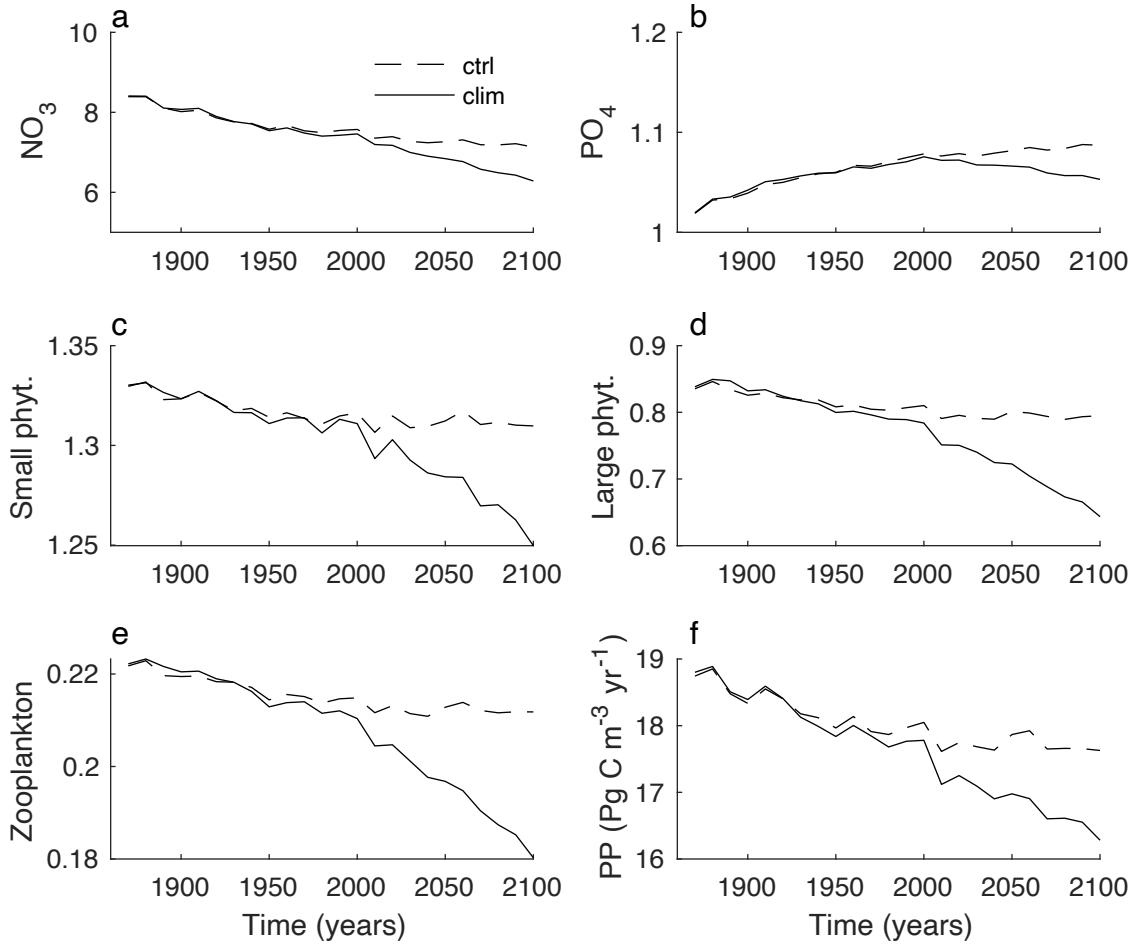

Fig. S7: Modeled marine biogeochemical tracers. Global mean concentrations of (**a**) dissolved nitrate (NO_3), (**b**) dissolved phosphate (PO_4), (**c**) small phytoplankton organic carbon, (**d**) large phytoplankton organic carbon, (**e**) zooplankton organic carbon, and (**f**) primary productivity (PP; Pg C m^{-3} yr^{-1}). All tracers, except PP, are reported in mmol m^{-3}. Dashed and solid lines show control simulation (Phase 2; Methods) and high emission scenarios (Phases 3–4), respectively.

Table S1. Literature compilation of in situ measurements of carbohydrates, proteins and lipids collected from the photic zone. The values in the table represent 5th–95th percentiles (median) of the samples collected in the photic zone. For ratios with fewer than three observations, raw values are displayed. *n* is the number of individual sampling points.

	#	*Sampling Location*	*Sampling Time*	*Carb-C:C*	*Protein-C:C*	*Lipid-C:C*	*n*	*Refs.*
Arctic Ocean	1	Labrador Sea	Sep 1978	0.28–0.46(0.42)	0.06–0.37(0.13)	0.28–0.46(0.42)	27	Irwin et al., 1980[45]
	2	Can. Arctic	July-Oct,1979	0.16–0.39(0.30)	0.20–0.61(0.37)	0.16–0.39(0.30)	82	Irwin et al., 1984[46]
	3	Can. Arctic	July-Aug,1980	0.11–0.42(0.20)	0.14–0.74(0.57)	0.11–0.42(0.20)	16	Irwin et al., 1983a[47]
	4	Can. Arctic	Aug-Sep,1981	0.18–0.42(0.33)	0.13–0.62(0.32)	0.18–0.42(0.33)	11	Irwin et al., 1983b[48]
	5	N. Atlantic	July-Aug,1980	0.16–0.48(0.30)	0.22–0.52(0.38)	0.11–0.26(0.18)	**35**	**Li and Platt, 1982**[44]
	6	N.E. Greenland	May-July, 1993	0.36, 0.39	0.34, 0.42	0.11, 0.11	**2**	**Smith et al., 1997**[49]
	7	Chukchi Sea	Aug, 2004	0.05–0.20(0.05)	0.21–0.85(0.60)	0.02–0.08(0.04)	**15**	**Lee et al., 2009**[50]
	8	Chukchi Sea	July-Aug, 2011	0.12–0.43(0.21)	0.01–0.35(0.10)	0.46–0.79(0.62)	42	Kim et al., 2015[51]
	9	Chukchi sea	Aug-Sep, 2012	0.11–0.23(0.16)	0.07–0.25(0.12)	0.60–0.78(0.71)	25	Yun et al., 2015[11]
	10	Laptev Sea	Aug-Sep, 2013	0.16–0.48(0.35)	0.19–0.53(0.41)	0.20–0.36(0.27)	37	Ahn et al.., 2019[72]
	11	Chukchi sea	July-Aug, 2014	0.19–0.67(0.37)	0.03–0.36(0.17)	0.22–0.71(0.38)	63	Choe et al., 2021[52]
	12	Chukchi Sea	Aug, 2017	0.06–0.16(0.12)	0.16–0.44(0.25)	0.45–0.73(0.65)	12	Kim et al., 2020[53]
Antarctic Ocean	13	S. Ocean	Sep-Oct, 1987	0.08–0.84(0.49)	0.03–0.27(0.11)	0.04–0.89(0.37)	**8**	**Smith and Morris, 1980**[43]
	14	S. Pacific	1980-1981	0.11–0.13(0.12)	0.34–0.40(0.37)	0.22–0.31(0.23)	3	Handa and Tanoue 1983[30]
	15	Ross Sea	Nov 1989 – Jan 1990	0.18–0.54(0.27)	0.35–0.71(0.59)	0.08–0.16(0.11)	10	Fabiano et al., 1993[54]
	16	Ross Sea	Jan-Feb, 1990	0.17, 0.20	0.60, 0.64	0.16, 0.22	2	Fabiano et al., 1996[55]
	17	Ross Sea	Jan-Feb, 1995	0.20–0.25(0.24)	0.46–0.59(0.52)	0.18–0.29(0.25)	6	Fabiano and Pusceddu 1998[56]
	18	Ross Sea*	Jan, 1995	0.03–0.12(0.08)	0.34–0.56(0.43)	0.34–0.57(0.45)	15	Puseceddu et al., 1999[57]
	19	Amundsen Sea	Feb-March, 2012	0.09–0.26(0.17)	0.52–0.77(0.68)	0.08–0.32(0.13)	14	Kim et al., 2016[58]
	20	Amundsen Sea	March-Nov, 2014	0.20–0.54(0.36)	0.25–0.48(0.37)	0.12–0.41(0.26)	21	Kim et al., 2018[10]
	21	Ross Sea	Jan-Feb 2017	0.26–0.39(0.35)	0.43–0.55(0.50)	0.13–0.19(0.17)	4	Misic et al., 2024[59]
	22	Ross Sea	Feb, 2018	0.23–0.52(0.43)	0.05–0.26(0.15)	0.36–0.55(0.41)	18	Jo et al., 2021[60]
Japan Sea	23	Japan Sea	Oct, Apr, 2012	0.16–0.49(0.30)	0.20–0.36(0.26)	0.24–0.60(0.44)	21	Kang et al., 2017[89]
	24	Japan Sea	Apr-Nov, 2014	0.27–0.59(0.41)	0.10–0.49(0.18)	0.18–0.62(0.34)	8	Jo et al., 2017[90]
	25	Japan Sea	May-Oct, 2015	0.28–0.47(0.43)	0.12–0.22(0.13)	0.35–0.58(0.40)	5	Jo et al., 2018[91]
	26	Japan Sea	Apr, 2016	0.05–0.46(0.30)	0.05–0.34(0.16)	0.29–0.82(0.54)	38	Kang et al., 2020[92]
Other Regions	27	S. Korea	Jun 2012 -Apr 2013	0.10–0.31(0.18)	0.11–0.69(0.33)	0.22–0.71(0.48)	45	Lee et al., 2017[93]
	28	S. Korea	Jan-Dec 2015	0.21–0.48(0.36)	0.15–0.37(0.30)	0.25–0.52(0.34)	12	Kim et al., 2018b[94]
	29	Yellow Sea	Apr 2015-Nov 2016	0.32–0.64(0.49)	0.06–0.33(0.21)	0.19–0.53(0.31)	54	Lee et al., 2020[95]
	30	Mediterranean	Aug1994-Sep 1995	0.20–0.54(0.33)	0.23–0.51(0.34)	0.16–0.52(0.32)	102	Danovaro et al., 2000[96]
	31	Mediterranean	May, July, 2001	0.05–0.29(0.21)	0.36–0.57(0.47)	0.21–0.83(0.52)	8	Modica et al., 2006[97]
	32	Baltic Sea	Apr-Sep, 1988	0.15–0.46(0.27)	0.18–0.62(0.39)	0.09–0.38(0.14)	**24**	**Lindqvist and Lingell 1997**[98]
	33	N. Atlantic	Apr, 1969	0.17–0.73(0.47)	0.31–0.57(0.40)	0.14–0.42(0.35)	**10**	**Platt and Irwin, 1973**[42]
	34	N. Atlantic	June-Oct, 1976	0.20–0.31(0.23)	0.56–0.68(0.62)	0.11–0.17(0.13)	8	Mayzaud and Taguchi 1979[99]
	36	N. Atlantic	Apr-May, 1979	0.23–0.45(0.40)	0.08–0.48(0.16)	0.23–0.45(0.40)	53	Irwin et al., 1983c[100]
	37	N. Atlantic	Jul-Oct, 1979	0.23–0.44(0.38)	0.09–0.51(0.21)	0.23–0.44(0.38)	54	Irwin et al., 1984[46]
	38	N. Atlantic	July, 1980	0.14–0.35(0.23)	0.27–0.68(0.50)	0.14–0.35(0.23)	6	Irwin et al., 1983a[47]
	39	N. Atlantic	May, 1981	0.37–0.48(0.44)	0.03–0.24(0.10)	0.37–0.48(0.44)	23	Irwin et al., 1983d[101]
	40	N. Atlantic	July, 1982	0.22–0.44(0.36)	0.10–0.54(0.25)	0.22–0.44(0.36)	26	Irwin et al., 1983e[102]
	41	N.E. Atlantic	July 2010-May 2011	0.15–0.20(0.16)	0.48–0.55(0.52)	0.28–0.36(0.30)	8	Fernández-Reiriz, 2017[103]
	42	N.E. Atlantic	Apr-July, 2000	0.03–0.13(0.06)	0.40–0.88(0.68)	0.06–0.57(0.24)	18	Diaz et al 2007[104]
	43	N. Pacific	June, 2017	0.18–0.38(0.25)	0.24–0.50(0.40)	0.23–0.35(0.26)	12	**Liefer et al., 2024[27]
	44	Pacific	1968	0.16–0.33(0.21)	0.21–0.55(0.36)	-	22	**Handa 1973[29]
	45	E. Eq. Pacific	Jan-Feb, 2006	0.19–0.31(0.28)	0.17–0.37(0.21)	0.33–0.63(0.51)	8	Isla et al., 2010[105]
	46	E. Eq. Pacific	Feb, July 2006, 2007	0.08–0.32(0.18)	0.17–0.53(0.39)	0.37–0.51(0.44)	4	Isla et al., 2012[106]
	47	Magellan Strt.	Feb-March, 1991	0.12–0.17(0.15)	0.35–0.55(0.46)	0.21–0.51(0.31)	7	Fabiano et al., 1999[107]

*Sea ice samples[57].

**Open ocean samples.

Bold references used isotope labelling techniques, which measure photosynthetic carbon allocation in living phytoplankton.

Table S2. Statistical analyses of the observations at the different ecoprovinces.

Region	CN_{nob}	CN_{out}	CN_{25}	CN_{50}	CN_{75}	CP_{nob}	CP_{out}	CP_{25}	CP_{50}	CP_{75}	NP_{nob}	NP_{out}	NP_{25}	NP_{50}	NP_{75}
NP—SPSS	1144	40	5.9	6.7	8.0	64	3	96	139	182	64	1	12	16	19
NP—STPS	1206	18	5.7	6.3	7.1	1342	57	122	152	196	1342	52	18	23	30
NP—STSS	2989	69	5.9	6.6	7.4	-	-	-	-	-	-	-	-	-	-
PEQU—W	158	4	6	6.8	8.1	22	-	102	133	209	21	1	14	15	24
PEQU—E	839	43	5.8	6.6	8.1	349	20	105	123	148	384	8	14	18	22
SP— STPS	718	6	6.1	7.3	9.0	369	18	141	189	259	445	19	18	22	28
NA—SPSS	201	4	6.3	7.2	8.9	32	1	107	120	149	30	2	7	12	14
NA—STSS	1109	9	6.7	8.6	10.9	268	12	137	162	200	264	10	18	23	27
NA—STPS	3100	97	5.3	6.6	8.4	1513	36	121	166	212	1625	30	17	25	34
AEQU	141	9	6.4	7.2	8.5	42	2	139	152	177	42	3	22	24	26
SA—STPS	588	2	6.8	7.5	8.9	307	1	141	155	174	307	7	20	23	25
IND—STPS	948	37	6.0	6.6	7.2	848	28	111	124	140	848	27	17	19	20
SO—STSS	488	21	5.9	6.6	7.7	191	11	109	119	132	191	10	18	20	22
SO—SPSS	1383	69	6.0	6.9	8.4	95	2	58	75	112	95	2	10	12	19

The observations are from the upper 170 m depth. CN_{nob}, CP_{nob}, NP_{nob} represent the number of observations at each ecoprovince. $CN_{out,}$ CP_{out}, NP_{out} are the outliers excluded from the mean (mean$\pm$2 standard deviations). CN_{25}, CN_{50}, CP_{25}, CP_{50}, CP_{75} and NP_{25}, NP_{50}, NP_{75} are the 25th, 50th, and 75th percentiles of the $C:N_{org}$, $C:P_{org}$ and $N:P_{org}$ observed data in each ecoprovince, respectively (molar ratios).

Table S3. Modeled $C:N_{org}$, $C:P_{org}$ and $N:P_{org}$ means from the global macromolecular model.

Region	CN'$_{nob}$	CN'25	CN'50	CN'75	CP'$_{nob}$	CP'25	CP'50	CP'75	NP'$_{nob}$	NP'25	NP'50	NP'75
NP—SPSS	282	4.6	4.8	5.2	284	93	97	105	284	19	20	22
NP—STSS	111	5.6	5.8	6.2	-	-	-	-	-	-	-	-
NP—STPS	667	6.9	7.4	7.6	667	151	160	165	667	21	22	22
PEQU—W	176	7.1	7.3	7.6	176	160	164	167	176	21	21	22
PEQU—E	236	6.6	6.9	7.2	236	137	139	145	236	20	20	21
SP— STPS	938	6.6	7.4	7.7	938	150	166	170	938	21	22	24
NA—SPSS	298	4.8	5.0	5.3	298	84	86	92	298	18	19	20
NA—STSS	98	5.5	5.5	5.7	98	106	108	110	98	19	19	20
NA—STPS	312	5.9	6.7	7.4	312	122	142	158	312	18	19	22
AEQU	101	10.5	11.7	12.4	101	119	122	127	101	10	10	11
SA—STPS	299	6.8	7.5	8.7	299	127	141	157	299	16	19	22
IND—STPS	588	7.1	8.3	10.2	588	126	136	147	588	12	16	21
SO—STSS	564	4.7	4.9	5.2	564	102	110	119	564	22	23	24
SO—SPSS	742	4.1	4.3	4.4	742	91	95	102	742	22	23	23

CN'$_{nobs}$, CP'$_{nobs}$, NP'$_{nobs}$ represent the number of modeled values at each ecoprovinces. CN'25th, CN'50th, CN'75th, CN'25th, CN'50th, CP'75th and NP'25th, NP'50th, NP'75th are the 25th, 50th, and 75th percentiles of the $C:N_{org}$, $C:P_{org}$ and $N:P_{org}$ modeled data in each ecoprovince, respectively (molar ratios).

Table S4. Comparison between the model and observed $C:N_{org}$, $C:P_{org}$, and $N:P_{org}$.

Region	$\mu_{CN,obs}$	$\mu_{CN,model}$	Δ_{CN}	σ_{CN}	$\mu_{CP,obs}$	$\mu_{CP,model}$	Δ_{CP}	σ_{CP}	$\mu_{NP,obs}$	$\mu_{NP,model}$	Δ_{NP}	σ_{NP}
NP—SPSS	6.9	4.9	0.349	30	138	100	0.677	27	15	20	0.718	27
NP—STSS	6.4	5.9	0.308	8	-	-	-	-	-	-	-	-
NP—STPS	6.7	7.3	0.276	8	156	153	0.471	1	23	21	0.504	10
PEQU—W	7.5	7.4	0.628	2	145	161	0.698	11	18	21	0.615	19
PEQU—E	6.9	6.9	0.398	0	129	140	0.527	8	18	20	0.614	11
SP— STPS	7.7	7.0	0.370	8	194	156	0.606	19	23	22	0.475	3
NA—SPSS	8.0	5.1	0.721	37	126	89	0.621	29	10	19	0.853	89
NA—STSS	8.7	5.6	0.642	35	170	108	0.809	34	22	19	0.886	11
NA—STPS	6.9	6.7	0.378	3	154	138	0.639	10	24	20	0.605	16
AEQU	7.5	11.3	0.089	50	164	123	0.454	25	24	11	0.105	56
SA—STPS	8.2	7.8	0.245	5	161	139	0.372	13	22	18	0.048	19
IND—STPS	6.6	8.4	0.140	28	125	134	0.181	7	19	16	0.193	16
SO—STSS	7.0	5.0	0.225	29	119	109	0.179	8	20	22	0.156	12
SO—SPSS	7.3	4.3	0.423	41	77	98	0.648	27	13	23	0.640	75
Σ			**5.1898***	**284***			**6.8831***	**221***			**6.4136***	**364***

$\mu_{CN,obs}$, $\mu_{CP,obs}$ and $\mu_{NP,obs}$ represent the means of the log-transformed distributions of the observed $C:N_{org}$, $C:P_{org}$ and $N:P_{org}$ ratios, respectively, in each ecoprovince (molar ratios). Similarly, $\mu_{CN,model}$, $\mu_{CP,model}$ and $\mu_{NP,model}$ denote the means of the log-transformed distributions of the modeled $C:N_{org}$, $C:P_{org}$ and $N:P_{org}$ ratios, respectively, in each ecoprovince. Δ represents the maximum difference between the cumulative distribution functions of the observed and modeled log-transformed $C:N_{org}$, $C:P_{org}$ and $N:P_{org}$, as determined by the Kolmogorov-Smirnov test. σ (%) is the relative distance between the modeled and observed distribution means, calculated using Eq. S1. Σ is the sum of the distances in all ecoprovinces.

Table S5. Linear regression results for temporal trends in polar phytoplankton macromolecules. Temporal trends in protein and carbohydrate + lipid concentrations were evaluated using ordinary least squares linear regression against time. Statistical significance was assessed using a two-sided test of the regression slope against zero. The table reports the number of observations, number of excluded outliers, slope estimates, P values and R^2. Only data obtained with colorimetric methods are included.

Region	***Regression***	***#Observations***	***#Outliers***	***Slope***	***p-value***	***R²***
Arctic	Protein vs. year	307	5	–0.0038	1.68×10^{-12}	0.156
Arctic	Carb + lipid vs. year	302	10	0.0041	2.52×10^{-15}	0.189
Antarctic	Protein vs. year	85	8	–0.0037	0.00941	0.078
Antarctic	Carb + lipid vs. year	93	0	0.0076	4.41×10^{-7}	0.246

Table S6. Linear regression results for temporal trends in polar phytoplankton macromolecules. Temporal trends in protein and carbohydrate + lipid concentrations were evaluated using ordinary least squares linear regression against time. Statistical significance was assessed using a two-sided test of the regression slope against zero. The table reports the number of observations, number of excluded outliers, slope estimates, P values and R^2. All data are included.

Region	*Regression*	*#Observations*	*#Outliers*	*Slope*	*p-value*	*R^2*
Arctic	Protein vs. year	359	5	–0.0037	4.2×10^{-12}	0.126
Arctic	Carb + lipid vs. year	342	22	0.0054	1.1×10^{-24}	0.266
Antarctic	Protein vs. year	96	5	–0.0020	0.143	0.022
Antarctic	Carb + lipid vs. year	101	0	0.0018	0.214	0.015

Table S7. Variables in the macromolecular model.

Symbol	Definition	Units
$Q_{\mathrm{C}}^{\mathrm{Pro}}$	Cellular carbon in proteins (all)	mol C (mol C)$^{-1}$
$Q_{\mathrm{C}}^{\mathrm{Pro-photo}}$	Cellular carbon in photosynthetic proteins	mol C (mol C)$^{-1}$
$Q_{\mathrm{C}}^{\mathrm{Pro-bio}}$	Cellular carbon in biosynthetic proteins	mol C (mol C)$^{-1}$
$Q_{\mathrm{C}}^{\mathrm{Pro-other}}$	Cellular carbon in essential proteins	mol C (mol C)$^{-1}$
$Q_{\mathrm{C}}^{\mathrm{RNA}}$	Cellular carbon in RNA	mol C (mol C)$^{-1}$
$Q_{\mathrm{C}}^{\mathrm{DNA}}$	Cellular carbon in DNA	mol C (mol C)$^{-1}$
$Q_{\mathrm{C}}^{\mathrm{Chl}}$	Chlorophyll to carbon ratio	mol C in Chl (mol C)$^{-1}$
$Q_{\mathrm{C}}^{\mathrm{PLip}}$	Cellular carbon in thylakoid lipids	mol C (mol C)$^{-1}$
$Q_{\mathrm{C}}^{\mathrm{Stor}}$	Carbon stored as carbohydrates and lipids	mol C (mol C)$^{-1}$
$Q_{\mathrm{C}}^{\mathrm{Other}}$	Fixed pool of carbon in carbohydrates and lipids	mol C (mol C)$^{-1}$
$Q_{\mathrm{N}}^{\mathrm{RNA}}$	Cellular nitrogen allocated to RNA	mol N (mol C)$^{-1}$
$Q_{\mathrm{N}}^{\mathrm{DNA}}$	Cellular nitrogen allocated to DNA	mol N (mol C)$^{-1}$
$Q_{\mathrm{N}}^{\mathrm{Chl}}$	Cellular nitrogen in chlorophyll	mol N (mol C)$^{-1}$
$Q_{\mathrm{N}}^{\mathrm{NStor}}$	Cellular nitrogen storage as cyanophycin	mol N (mol C)$^{-1}$
$Q_{\mathrm{P}}^{\mathrm{RNA}}$	Cellular phosphorous in RNA	mol P (mol C)$^{-1}$
$Q_{\mathrm{P}}^{\mathrm{Thy}}$	Cellular phosphorus in the thylakoid membrane	mol P (mol C)$^{-1}$
$Q_{\mathrm{P}}^{\mathrm{Stor}}$	Cellular phosphorus storage	mol P (mol C)$^{-1}$
$Q_{\mathrm{P}}^{\mathrm{Other}}$	Fixed pool of phosphorus	mol P (mol C)$^{-1}$
$Q_{\mathrm{Fe}}^{\mathrm{Pho}}$	Cellular iron in photosynthetic proteins	mol Fe (mol C)$^{-1}$
$Q_{\mathrm{Fe}}^{\mathrm{Stor}}$	Cellular iron storage	mol Fe (mol C)$^{-1}$

Table S8. Allometric relationships between cell volume and parameters.

Parameter	Description (units)
$\boldsymbol{V_j^{max,P} = 0.077V^{-0.27}}$	Maximum uptake rate (mmol P/mmol C/day)
$\boldsymbol{V_j^{max,N} = 0.51V^{-0.27}}$	Maximum uptake rate (mmol N/mmol C/day)
$\boldsymbol{V_j^{max,Fe} = 14 \times 10^{-6}V^{-0.27}}$	Maximum uptake rate (mmol Fe/mmol C/day)
$\boldsymbol{k_j^{P} = 0.026V^{0.27}}$	Half saturation constant (mmol P/m^3)
$\boldsymbol{k_j^{N} = 0.17V^{0.27}}$	Half saturation constant (mmol N/m^3)
$\boldsymbol{k_j^{Fe} = 80 \times 10^{-6}V^{0.27}}$	Half saturation constant (mmol Fe/m^3)

$V_{\mathrm{small}} = 0.41$ and $V_{\mathrm{large}} = 46.0$, where V is phytoplankton cell volume (μm^3).

Table S9. Stoichiometric parameters and constant that are used in the macromolecular model.

Parameter	Description	Value	Units
$Y_{\mathrm{Pro}}^{\mathrm{C:N}}$	C:N in proteins	5.3/1.4	mol C (mol N)$^{-1}$
$Y_{\mathrm{Nsto}}^{\mathrm{C:N}}$	C:N in N-storage as cyanophycin	2	mol C (mol N)$^{-1}$
$Y_{\mathrm{DNA}}^{\mathrm{P:C}}$	P:C in DNA	1/9.75	mol P (mol C)$^{-1}$
E	Respiratory costs of synthesis	0.774*	unitless
m	Maintenance respiration rate	0.393*	day^{-1}
V_I^{max}	Per-chloroplyll maximum photosynthesis rate	277*	mol C (mol C in Chl)$^{-1}$ day^{-1}
A_I	Absorption cross-section of the photosyn. unit	8.63×10^{-3}*	m^2 s µmol^{-1}
A_{Pho}	Proteins : Chl in the photosynthetic machinery	16*	mol C (mol C in Chl)$^{-1}$
$A_{\mathrm{Pho}}^{\mathrm{P:Chl}}$	P in thylakoid : Chl in the photosynthetic machinery	2.8163×10^{-2}*	mol P (mol C in Chl)$^{-1}$
$A_{\mathrm{Pho}}^{\mathrm{Fe:Chl}}$	Fe in thylakoid : Chl in the photosynthetic machinery	5.83×10^{-3}*	mol Fe (mol C in Chl)$^{-1}$
A_{bio}	Linear relationship between biosyn. proteins and growth	0.2711*	mol C (mol C)$^{-1}$day
$A_{\mathrm{P}}^{\mathrm{RNA}}$	A constant of proportionality between RNA and proteins	4.23×10^{-3}*	mol P (mol C)$^{-1}$ day
$Q_{\mathrm{P,min}}^{\mathrm{RNA}}$	Minimum RNA in the cell	2.23×10^{-4}*	mol P (mol C)$^{-1}$
$Q_{\mathrm{P}}^{\mathrm{Other}}$	Fixed pool of phosphorus	6.5344×10^{-4}*	mol P (mol C)$^{-1}$
$Q_{\mathrm{C}}^{\mathrm{Pro-other}}$	Cellular carbon in essential proteins	0.24*	mol C (mol C)$^{-1}$
$Q_{\mathrm{C}}^{\mathrm{Other}}$	Fixed pool of carbon in carbohydrates and lipids	0.0182*	mol C (mol C)$^{-1}$
$Q_{\mathrm{C}}^{\mathrm{DNA}}$	Fixed pool of cellular carbon in DNA	9.41×10^{-4}*	mol C (mol C)$^{-1}$
$Q_{\mathrm{z}}^{\mathrm{P,max}}$	Maximum grazer phosphorous quota	0.008	mol P (mol C)$^{-1}$
$Q_{\mathrm{z}}^{\mathrm{P,min}}$	Minimum grazer phosphorous quota	0.010	mol P (mol C)$^{-1}$
$Q_{\mathrm{z}}^{\mathrm{N,max}}$	Maximum grazer nitrogen quota	0.1	mol N (mol C)$^{-1}$
$Q_{\mathrm{z}}^{\mathrm{N,min}}$	Minimum grazer nitrogen quota	0.2	mol N (mol C)$^{-1}$
$Q_{\mathrm{z}}^{\mathrm{Fe,max}}$	Maximum grazer iron quota	2×10^{-5}	mol Fe (mol C)$^{-1}$
$Q_{\mathrm{z}}^{\mathrm{Fe,min}}$	Minimum grazer iron quota	1×10^{-6}	mol Fe (mol C)$^{-1}$

*These constants were originally tuned to simulate stoichiometry and growth of the cyanobacteria *Synechococcus linearis* in the original study that developed the macromolecular model[23], and in the study that embedded the macromolecular model in the Darwin package in the MITgcm[25].

Supplementary References:

89. Kang, J. J. *et al.* Comparison of biochemical compositions of phytoplankton during spring and fall seasons in the northern East/Japan Sea. *Deep Sea Res. Part II Top. Stud. Oceanogr.* **143**, 73–81 (2017).

90. Jo, N. *et al.* Seasonal variation in the biochemical compositions of phytoplankton and zooplankton communities in the southwestern East/Japan Sea. *Deep Sea Res. Part II Top. Stud. Oceanogr.* **143**, 82–90 (2017).

91. Jo, N. *et al.* Carbohydrate-dominant phytoplankton and protein-high zooplankton in the northern part of the Southwestern East/Japan Sea in 2015. *J. Coast. Res.* **85**, 371–375 (2018).

92. Kang, J. J. *et al.* Characteristics of different size phytoplankton for primary production and biochemical compositions in the Western East/Japan Sea. *Front. Microbiol.* **11**, 560102 (2020).

93. Lee, J. H. *et al.* The effects of different environmental factors on the biochemical composition of particulate organic matter in Gwangyang Bay, South Korea. *Biogeosciences* **14**, 1903–1917 (2017).

94. Kim, H. C. *et al.* Decoupling of macromolecular compositions of particulate organic matters between the water columns and the sediment in Geoje-Hansan Bay, South Korea. *Ocean Sci. J.* **53**, 735–743 (2018).

95. Lee, J. H. *et al.* Major controlling factors for spatio-temporal variations in the macromolecular composition and primary production by phytoplankton in Garolim and Asan bays in the Yellow Sea. *Reg. Stud. Mar. Sci.* **36**, 101269 (2020).

96. Danovaro, R. *et al.* Biochemical composition of pico-, nano- and micro-particulate organic matter and bacterioplankton biomass in the oligotrophic Cretan Sea (NE Mediterranean). *Prog. Oceanogr.* **46**, 279–310 (2000).

97. Modica, A., Scilipoti, D., La Torre, R., Manganaro, A. & Sarà, G. The effect of mariculture facilities on biochemical features of suspended organic matter (southern Tyrrhenian, Mediterranean). *Estuar. Coast. Shelf Sci.* **66**, 177–184 (2006).

98. Lindqvist, K. & Lignell, R. Intracellular partitioning of 14CO2 in phytoplankton during a growth season in the northern Baltic. *Mar Ecol Prog Ser* **152**, 41–50 (1997).

99. Mayzaud, P. & Taguchi, S. Spectral and biochemical characteristics of the particulate matter in Bedford Basin. *J. Fish. Res. Board Can.* **36**, 211–218 (1979).

100. Irwin, B., Lindley, P., Gallegos, C. L. & Platt, T. Phytoplankton productivity experiments, on the Scotian Shelf from April 18 to May 2, 1979. *Can. Data Rep. Fish. Aquat. Sci.* **384**, 118 (1983).

101. Irwin, B., Platt, T., Lindley, P., Fasham, M. J. & Jones, K. Phytoplankton productivity in the vicinity of a front, S.W. of the Azores during May 1981. *Can. Data Rep. Fish. Aquat. Sci.* **400**, 101 (1983).

102. Irwin, B., Caverhill, C., Subba Rao, D. V., Carver, V. & Platt, T. Primary productivity measurements in the chlorophyll maximum in the vicinity of the Mid-Atlantic Ridge, west of the Azores, from 8 July to 25 July, 1982. *Can. Data Rep. Fish. Aquat. Sci.* **402**, 84 (1983).

103. Fernández-Reiriz, M. J., Labarta, U. & Zúñiga, D. Bioavailable organic matter in seston modulating differential absorption rates by mussels. *Aquaculture* **479**, 161–168 (2017).

104. Díaz, E., Valencia, V. & Villate, F. Size-fractionated seston abundance and biochemical composition, over the anchovy spawning period in the Basque shelf (Bay of Biscay), during years 2000 and 2001. *J. Exp. Mar. Biol. Ecol.* **341**, 45–59 (2007).

105. Isla, E. *et al.* Biochemical composition of seston in two upwelling sites within the Humboldt Current System (21°S to 23°S): Summer conditions. *J. Mar. Syst.* **82**, 61–71 (2010).

106. Isla, E., Sañé, E., Homs, P., Teixidó, N. & Escribano, R. Temporal variation of the concentration and biochemical composition of seston within the Humboldt Current System off northern Chile (21°S). *Chem. Ecol.* **28**, 123–140 (2012).

107. Fabiano, M., Povero, P., Danovaro, R. & Misic, C. Particulate organic matter composition in a semi enclosed periantarctic system: the Straits of Magellan. *Sci Mar* **63**, 89–98 (1999).

108. Geider, R. J. & LaRoche, J. Redfield revisited: variability of C:N:P in marine microalgae and its biochemical basis. *Eur J Phycol* **37**, 1–17 (2002).

109. MODIS. Global Level 3 Mapped SST. Ver. 1. PO.DAAC, CA, USA. (2022).

110. Garcia, H. *et al.* World Ocean Atlas 2018, Volume 3: Dissolved Oxygen, Apparent Oxygen Utilization, and Dissolved Oxygen Saturation. *NOAA Atlas NESDIS 83* 38 (2019).